AGU100 ADVANCING EARTH AND SPACE SCIENCE

Space Weather

RESEARCH ARTICLE
10.1029/2018SW001863

Key Points:
- Optimized ANN structure to forecast the *Dst* index
- Solar wind parameters were used for forecasting the *Dst* index 1 to 12 hr in advance
- Investigating the geoeffectiveness of the solar wind parameters

Supporting Information:
- Supporting Information S1
- Table S1
- Table S2
- Table S3
- Table S4
- Table S5
- Table S6
- Table S7
- Table S8
- Table S9
- Table S10
- Table S11
- Table S12

Correspondence to:
A. Lethy,
alethy@nriag.sci.eg

Citation:
Lethy, A., El-Eraki, M. A., Samy, A., & Deebes, H. A. (2018). Prediction of the *Dst* index and analysis of its dependence on solar wind parameters using neural network. *Space Weather*, *16*, 1277–1290. https://doi.org/10.1029/2018SW001863

Received 10 MAR 2018
Accepted 8 AUG 2018
Accepted article online 25 AUG 2018
Published online 6 SEP 2018

Prediction of the *Dst* Index and Analysis of Its Dependence on Solar Wind Parameters Using Neural Network

Ahmed Lethy[1], Mohamed A. El-Eraki[2], Aalaa Samy[1], and Hanafy A. Deebes[1]

[1]National Research Institute of Astronomy and Geophysics, Helwan, Egypt, [2]Faculty of Science, Zagazig University, Zagazig, Egypt

Abstract In this work, we propose an artificial neural network (ANN) with seven input parameters for the prediction of disturbance storm time (*Dst*) index 1 to 12 hr ahead. The ANN uses past near-Earth solar wind parameter values to forecast the *Dst*. The input parameters are the solar wind interplanetary magnetic field, north-south component of interplanetary magnetic field, temperature, density, speed, pressure, and electric field. The ANN was trained on the data period from 1 January 2007 to 31 December 2015, which contains 78,888 hourly data samples. While the period from 1 January 2016 to 31 May 2017 was used to test the prediction capabilities of the ANN. Several ANN structures were tested and the best results were determined using the correlation coefficient (*R*) during the training and prediction phases. The results indicate an adequate accuracy of $R = 0.876$ for prediction 2 hr in advance and $R = 0.857$ for prediction 12 hr in advance. The power of the proposed ANN was illustrated using the strongest six storms recorded during the prediction period. Generally, the duration and number of the input parameters significantly affect the training and prediction performance of the applied ANN. The results are outstanding in term of accuracy when considering a medium-term prediction of 12 hr in advance and in terms of timing of the *Dst* minimum occurrence. In addition, the results show a strong dependence on the solar wind electric current.

Plain Language Summary We propose an artificial neural network for the prediction of disturbance storm time (*Dst*) index 1 to 12 hr ahead. The ANN uses 24 past hourly solar wind parameters values to forecast the *Dst* index. The input parameters are the solar wind interplanetary magnetic field, southward component of interplanetary magnetic field, temperature, density, speed, pressure, and electric field. Several ANN structures were tested and the best results were determined using the correlation coefficient (*R*) during the training and prediction phases. The results indicate an adequate accuracy of $R = 0.876$ for prediction 2 hr in advance and $R = 0.857$ for prediction 12 hr in advance. Generally, the duration and number of the input parameters significantly affect the training and prediction performance of the applied ANN. The results are outstanding in term of accuracy when considering a medium-term prediction of 12 hr in advance and in term of timing of the *Dst* minimum occurrence. In addition, the results show a strong dependence on the solar wind electric current.

1. Introduction

The space weather and the solar-terrestrial relationship have been under investigation for a long time. Nowadays, geomagnetic storm forecasting is one of the main subjects of the space weather studies. Numerous efforts have been made during the last decades to find a relationship between solar and interplanetary phenomena and geomagnetic indices (Li et al., 2007; MacDonald & Ward, 1963; Uwamahoro & Habarulema, 2014). However, several authors focus their work on the prediction of the disturbance storm time (*Dst*) index (Caswell, 2014; Gonzalez et al., 2004; Kim et al., 2014; Mays et al., 2009; Qin & Nishii, 2015; Temerin & Li, 2002). Also, Ji et al. (2012) represent a comparison of different *Dst* models.

The *Dst* index measures the intensity of the globally symmetrical equatorial electrojet (ring current) that is caused by solar wind plasma ejecta and/or high-speed streams. The basic idea to the *Dst* index was first introduced by Sugiura and Chapman (1960). Later on, Sugiura (1964) published the hourly average value of the low-latitude horizontal (*H*) component of the Earth's magnetic field. The original formula for the *Dst* index calculation was described in Sugiura (1964, 1969), and Sugiura and Kamei (1991). The *Dst* index is hourly calculated using magnetic measurements from four ground-based low-latitude observatories which are Hermanus, Kakioka, Honolulu, and San Juan observatories (Masahito et al., 2015).

Several methods have been developed for *Dst* index forecasting using interplanetary magnetic field (IMF) and solar wind as input. Many authors have used statistical relations between the *Dst* index and the solar wind parameters (e.g., Gonzalez & Echer, 2005; Yermolaev et al., 2005; Yermolaev et al., 2010; Yermolaev & Yermolaev, 2002). Meanwhile, others deduced a coupling functions between the solar wind and the magnetosphere (e.g., Akasofu, 1981; Boynton et al., 2011; Burton et al., 1975; Nikolaeva et al., 2014; O'Brien & McPherron, 2000; Perreault & Akasofu, 1978). Rastätter et al. (2013) present review and detailed analysis of several statistical and physics-based model performance to calculate the *Dst* index.

Nevertheless, many attempts have been made to predict the *Dst* index using neural network (Kugblenu et al., 1999; Lazzús et al., 2014; Lundstedt & Wintoft, 1994; Pallocchia et al., 2006; Wu & Lundstedt, 1996, 1997). Using the past *Dst* values Lazzús et al. (2017) present artificial neural network (ANN) that can forecast the *Dst* index 1 to 6 hr ahead. Meanwhile, Gleisner et al. (1996) used solar wind density, velocity, and the southward component B_z of the interplanetary magnetic field to forecast the *Dst* index 1 hr in advance. Caswell (2014) used B_x, B_y, and B_z components of the IMF, solar wind proton density, solar wind plasma speed, and plasma flow pressure to predict the *Dst* index 1 hr in advance. Similarly, Watanabe et al. (2002) used the solar wind velocity, density, and IMF B_x, B_y, B_z, and B_t to predict the *Dst* index 2 hr in advance.

2. ANN Method

An artificial neuron network is a computational system inspired by the biological neural networks. The artificial neural network is composed of a number of interconnected units (neurons/nodes). Each unit has an input/output (I/O) characteristic and implements a local computational function that is usually the summation of the weighted inputs. The output of any unit is determined by its I/O characteristic, its interconnection to other units, and (possibly) external inputs (Schalkoff, 1997).

The most common neural network structure is formed of three layers, called input, hidden, and output layers. Each layer consists of one or more neurons. Each value from the input layer, Xi, is sent to all the hidden neurons. This is called a fully interconnected structure. The values entering hidden neurons are multiplied by weights, Wi (a set of predetermined numbers). The weighted inputs are then added to produce a single number. Before leaving the neurons, this number is passed through a mathematical activation function, which limits the output of the neuron (Smith, 1997).

No rules exist for determining the exact number of neurons in the hidden layer. However, Huang and Huang (1991) derived the bounds on the number of the hidden neurons. Huang and Babri (1998) showed that the upper limit of the number of neurons needed to reproduce exactly the desired outputs of the training samples is in the order of the number of training samples in the training set (t). Moreover, to keep the training problem constrained, the number of training samples should always be larger than the number of internal weights. Mirko and Christain (2000) showed that a total of neurons 10 is considered to be a good choice in practice. Classically, the best configuration is found by trial, starting with a small number of neurons.

In this work, we used feedforward networks, where the connections between the neurons are directed in one direction from the input layer to the output layer passing through the hidden layer. The output layer has a linear activation function while the hidden layer has a sigmoid activation function (Kosko, 1992) which helps stabilize the network (Poulton et al., 1992).

The training function used in this work is the Levenberg–Marquardt (Levenberg, 1944; Marquardt, 1963) which is based on the back propagation algorithm; for example, it uses older weights to compute new ones. The batch training technique was used with these training functions. In batch training, the network weights are not modified until all the training samples are passed to the network. The objective of the training function is to minimize the error between the calculated and observed *Dst* values using mean square error.

Performance of the ANNs is measured during the training and prediction phases. The performance is measured using root-mean-square error (RMSE), mean absolute error (MAE), and the correlation coefficient (R) between the calculated and the observed *Dst* data as follows:

$$\mathrm{RMSE} = \sqrt{\frac{\sum_{i=0}^{n} \left(Dst_i^{Cal} - Dst_i^{Real}\right)^2}{n}}, \tag{1}$$

$$\mathrm{MAE} = \frac{1}{n}\sum_{i=0}^{n}\left|Dst_i^{Cal} - Dst_i^{Real}\right|, \tag{2}$$

$$R = \frac{\Sigma_{i=0}^{n}\left(Dst_i^{Cal} - \overline{Dst^{Cal}}\right)\left(Dst_i^{Real} - \overline{Dst^{Real}}\right)}{\sqrt{\Sigma_{i=0}^{n}\left(Dst_i^{Cal} - \overline{Dst^{Cal}}\right)^2 \Sigma_{i=0}^{n}\left(Dst_i^{Real} - \overline{Dst^{Real}}\right)^2}}, \tag{3}$$

The ANN performance depends on the initial weights (Meen et al., 2015). Therefore, each ANN is trained 3 times on the same data and the average performance is presented as its performance.

3. Data Sets

The data sets for the period January 2007 to May 2017 (solar wind parameters and *Dst* index) have been obtained from OMNI database (King & Papitashvili, 2005) of the National Space Science Data Center of NASA. These data sets are hourly averages of the solar wind plasma and IMF data. Hourly average of *Dst* index is also available in OMNI web. The solar wind parameters are the interplanetary magnetic field (B), the north-south component of interplanetary magnetic field (B_z), the plasma temperature (T), the plasma density (D), the plasma speed (V), the plasma pressure (P), and the plasma electric field (E). The data set contains 91,296 hourly data starting from 00:30 UT on 1 January 2007 to 23:30 UT on 31 May 2017. The data period was selected to cover the available data of the solar cycle 24. However, the final *Dst* index was only available until the end of 2012. Meanwhile provisional *Dst* index is provided for the period (2012–2015), and afterword, it was Quick-look *Dst*.

The database was divided into two sets. Training set that starts from 00:30 UT on 1 January 2007 to 23:30 UT on 31 December 2015 which contains 78,888 hourly data points. The second set is the prediction set which starts from 00:30 UT on 1 January 2016 to 23:30 UT on 31 May 2017 containing 12,408 hourly data points.

The training set is divided into three subsets learning set (containing 70% of the training set), validation and test sets (each contains 15% of the training set). The learning set is used to update the ANN weights through the training function, while the validation set is used to stop the training process once the prediction error of the validation set starts to increase. Meanwhile, the test set is used to test the ANN capability to estimate the *Dst*. Despite that the test set is laying within the period of the learning set, it should be clear that both the prediction set and test set were not used during the training process. The ANN is trained using old data before 2016 and is used to predict a more recent data until May 2017.

The study period contains hundreds of geomagnetic storms. According to the International Service of Rapid Magnetic Variations (Curto et al., 2007; Mayaud, 1973) available at (http://isgi.unistra.fr/events_sc.php) which is part of the International Service of Geomagnetic Indices, there are 240 storm sudden commencements observed during the period from January 2007 to May 2017. By inspecting the *Dst* index with respect to the list of storm sudden commencement we found 55 moderate storms and 20 intense storms during the learning period. While the prediction period contains two intense storms and nine moderate storms. The moderate storms have a minimum *Dst* between −50 and −100 nT while intense storms have minimum $Dst \leq -100$ nT (Gonzalez et al., 1994). The occurrence of such storms could be clarified from the data histogram (Figure 1). Also, Yermolaev et al. (2013) analyze the standard and integral distribution functions of the geomagnetic storm minimal *Dst* values during the period 1963–2012. Watari (2017) detects 17 intense geomagnetic storms during the period 2009–2015.

4. Forecasting Model

In typical dynamic nonlinear input-output ANN type, two sets are involved: an input set $x(t)$ and an output/target set $y(t)$. Here we want to predict values of $y(t)$ from previous values of $x(t)$. This input/output model for a time series can be written as follows:

$$y(t+S) = f(x(t), x(t-1), \ldots, x(t-d)), \tag{4}$$

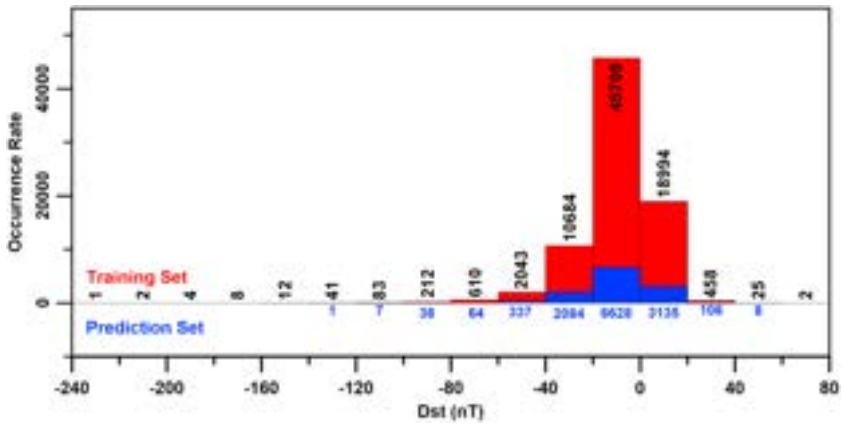

Figure 1. The *Dst* distribution of the training and prediction sets.

where d is the delay number representing the number of previous observations used and S is the time shift ahead into the future. This equation represents a prediction of y value ahead in the future at time $t + S$ using the past d values of x (t).

In our study, the aim is to predict the future *Dst* index value using past values of solar wind parameters $SW(t)$, which could simply be written as

$$Dst(t+S) = F(SW(t), SW(t-1), \ldots, SW(t-d)), \tag{5}$$

The prediction function F can be replaced by the ANN, which depends on the input solar wind parameters (SW), delay (d), shift (S), and the number of neurons in the hidden layer (N); then the prediction model can be rewritten as

$$Dst(t, N, S, d) = ANN[SW(t, d), N, S], \tag{6}$$

For simplicity, the time-dependent can be removed from equation (6):

$$Dst(N, S, d) = ANN[SW(d), N, S], \tag{7}$$

where the $SW(d)$ is the ANN input matrix constructed from the solar wind parameters in the form

$$\begin{pmatrix} B(t) & B_z(t) & T(t) & D(t) & V(t) & P(t) & E(t) \\ B(t-1) & B_z(t-1) & T(t-1) & D(t-1) & P(t-1) & V(t-1) & E(t-1) \\ \vdots & \vdots & \vdots & \vdots & \vdots & \vdots & \vdots \\ B(t-d) & B_z(t-d) & T(t-d) & D(t-d) & V(t-d) & P(t-d) & E(t-d) \end{pmatrix}, \tag{8}$$

5. Results

In order to select the most appropriate ANN structure, we test different numbers of neurons in the hidden layer with different time shift and delay. Figure 2 shows the values of the correlation coefficients for neural networks with a time delay from 1 to 9 hr and time shift from 0 to 6 hr with 5, 10, 15, 30, and 50 neurons in the hidden layer during the training phase. Generally, the values of the correlation coefficients increase with increasing the delay time (number of input samples) regardless of the time shift or the number of neurons. The results are enhanced at the shift of 2 hr and with increasing the delay number regardless of the number of neurons in the hidden layer (Figure 2f). The resulting enhancement at 2-hr time shift can be supported physically by the average time span between satellite observation and ground-based observations.

Meanwhile, increasing the delay increases the number of input samples and this multiplies the number of weights in the neural network and increases its capabilities. However, each weight update can reduce

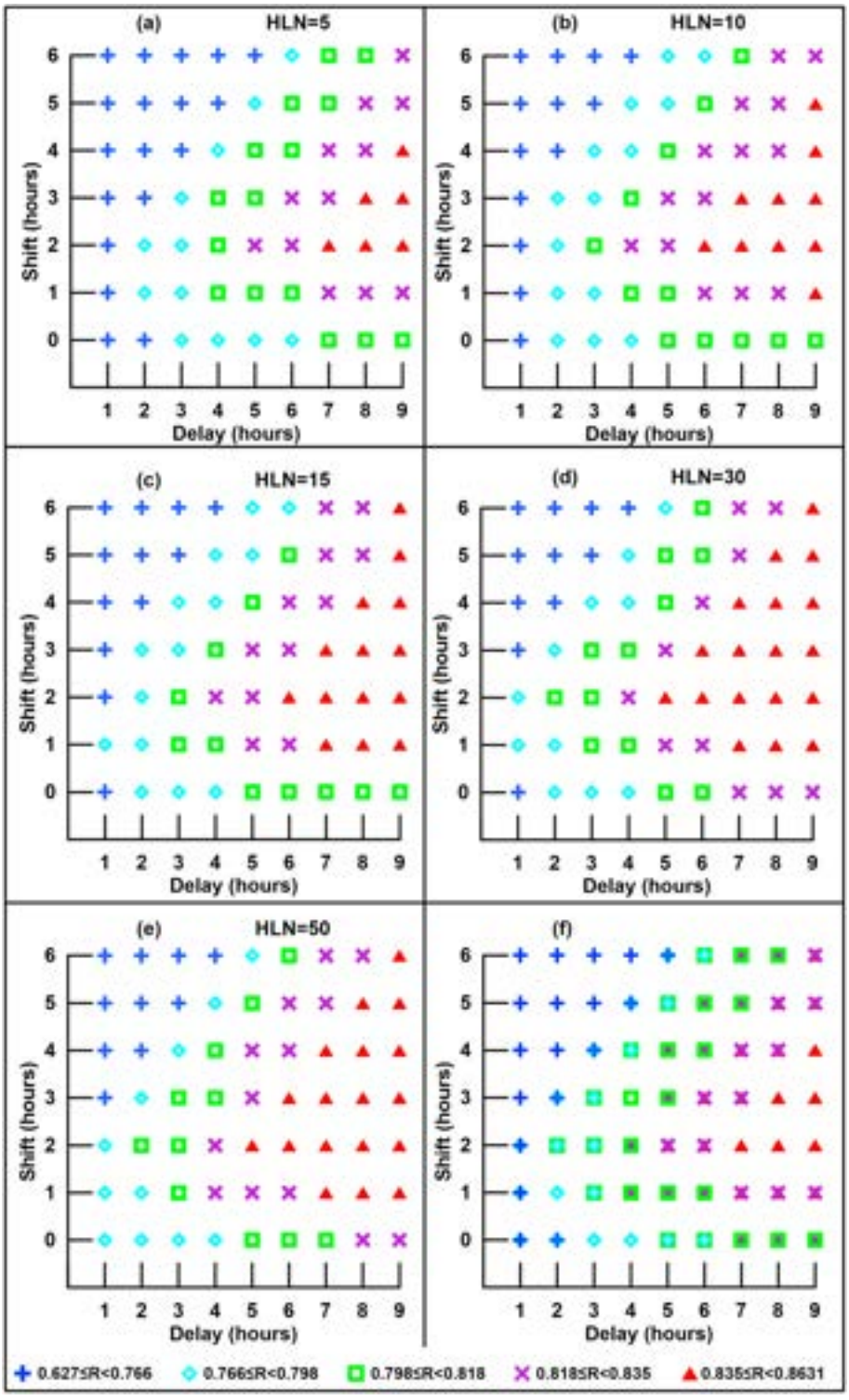

Figure 2. The values of the correlation coefficients between calculated and real *Dst* values for neural networks with a time delay from 1 to 9 hr and time shift from 0 to 6 hr with 5, 10, 15, 30, and 50 neurons in the hidden layer during the training phase. (a) The ANN has five neurons in the hidden layer (HLN = 5). (b) ANN has 10 neurons in the hidden layer. (c) HLN = 15 neurons. (d) HLN = 30. (e) HLN = 50. (f) Stack plot of the five panels (a–e). The correlation coefficient enhanced at the shift of 2 with increasing the delay time.

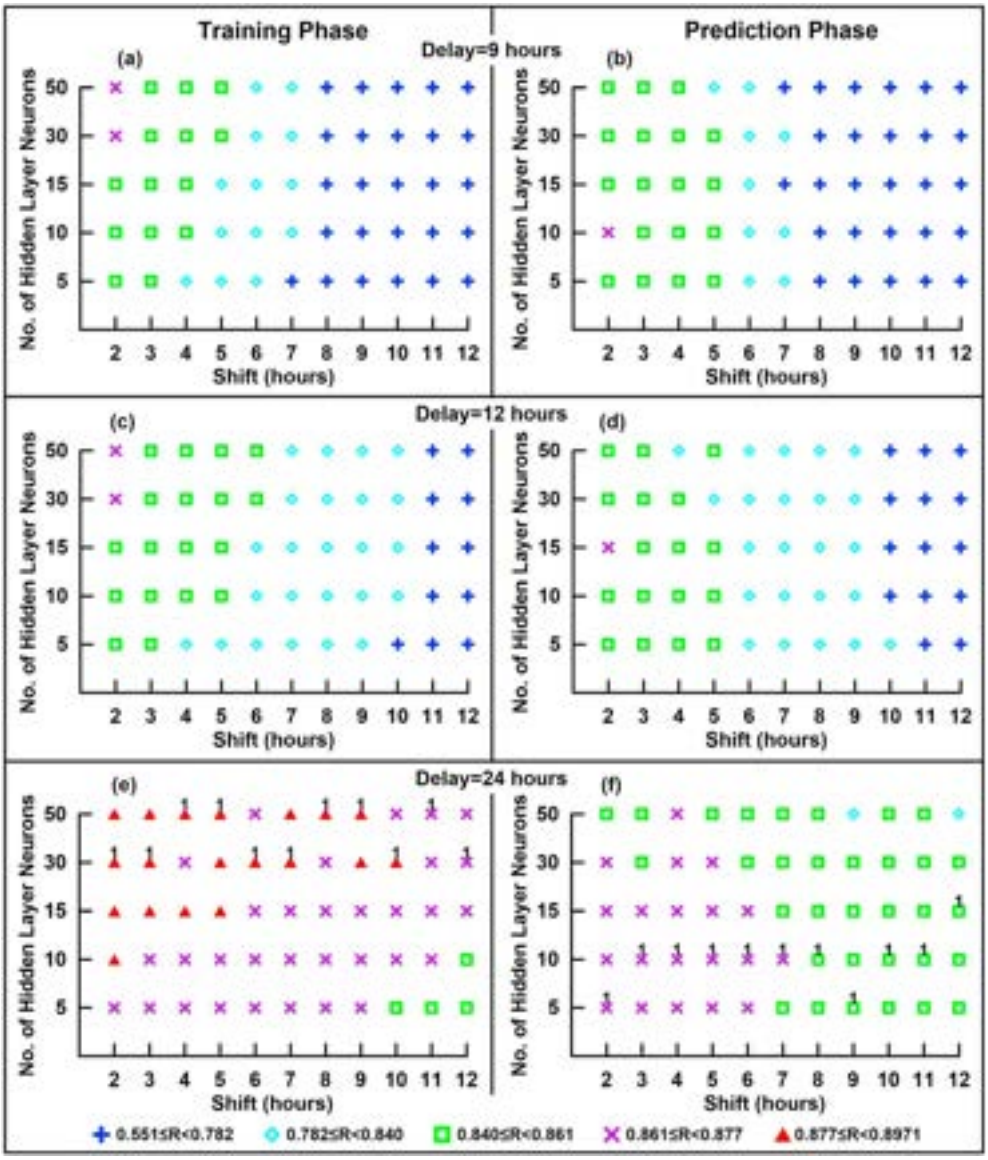

Figure 3. The performance measure (*R*) of ANNs with different numbers of neurons while forecasting the *Dst* 2 to 12 hr ahead using 9, 12, and 24 hr of past solar wind data. (a, c, and e) The ANN response during the training phase using delays of 9, 12, and 24 hr, respectively. (b, d, and f) The ANN response during the prediction phase using delays of 9, 12, and 24 hr, respectively. The highest performance at each time shift is marked with superscript (1) in (e) and (f).

error only slightly, so many iterations are required in order to minimize the error (Reed and Marks, 1999). Therefore, we increase the delay to 12 and 24 hr.

Figure 3 shows the correlation coefficients between the calculated and the real *Dst* values of the training and prediction sets for ANNs with delays of 9, 12, and 24 hr for a different number of neurons. Generally, the effectiveness of the forecast increases as the delay increases from 9 to 24 hr. Similarly, the performance during the training phase (Figures 3a, 3c, and 3e) increases with increasing the number of neurons. However, reduction in performance occurs during the prediction phase with increasing the number of neurons (Figure 3f). The highest performance at each time shift is marked with superscript (1) in Figures 3e and 3f. The statistical performance measures of these ANNs marked in Figures 3e and 3f are listed in Table 1. This indicates that the ANN has a poor generalization. This could be due to the large increase of the total number of weights in the ANN with increasing the number of neurons in the hidden layer. Lawrence and Giles (2000) show that the overfitting occurs when the total number of weights in the network is relatively large compared to the

Table 1
Performance of the ANNs Obtaining the Maximum R During Training and Prediction Phases for Shift From 1 to 12 hr

		Training phase								
		Training set			Learning	Validation	Test	Prediction phase		
HLN	Shift	RMSE (nT)	MAE (nT)	*R*	RMSE (nT)	RMSE (nT)	RMSE (nT)	RMSE (nT)	MAE (nT)	*R*
15	1	69.62	6.16	0.842	68.27	72.11	73.45	74.03	6.63	0.845
5	2	58.23	5.68	0.870	56.53	63.04	61.38	64.46	6.12	0.874
30	2	53.31	5.45	0.883	48.28	65.22	64.86	70.55	6.33	0.866
10	3	55.82	5.59	0.876	53.57	60.88	61.28	64.90	6.10	0.872
30	3	52.69	5.41	0.886	45.10	67.83	72.96	78.50	6.62	0.856
10	4	55.67	5.58	0.876	53.16	61.62	61.43	66.63	6.18	0.869
50	4	51.93	5.41	0.886	47.02	62.79	63.94	69.77	6.27	0.863
10	5	57.81	5.67	0.871	55.05	64.95	63.54	67.11	6.18	0.865
50	5	52.16	5.42	0.886	46.04	66.94	65.90	74.53	6.44	0.857
10	6	57.41	5.65	0.872	55.21	62.41	62.67	67.77	6.21	0.864
30	6	52.76	5.44	0.884	47.54	64.06	65.86	72.48	6.35	0.856
10	7	58.88	5.72	0.869	56.95	64.08	62.67	68.67	6.20	0.862
30	7	54.56	5.54	0.880	50.35	64.28	64.48	73.47	6.42	0.856
10	8	58.75	5.70	0.869	55.89	65.23	65.58	69.55	6.29	0.860
50	8	54.94	5.56	0.880	48.67	69.81	69.30	80.23	6.67	0.846
5	9	61.40	5.82	0.863	59.98	64.52	64.92	69.20	6.24	0.860
50	9	55.02	5.48	0.879	46.55	73.07	76.51	82.31	6.60	0.837
10	10	60.86	5.80	0.864	58.55	66.72	65.74	70.34	6.27	0.857
30	10	54.36	5.53	0.879	50.88	62.16	62.77	72.03	6.30	0.852
10	11	59.93	5.75	0.866	58.14	64.58	63.66	67.26	6.13	0.860
50	11	56.97	5.64	0.874	52.32	65.98	69.64	76.01	6.51	0.851
15	12	60.41	5.79	0.865	57.88	66.95	65.70	70.92	6.33	0.857
30	12	58.58	5.68	0.870	52.50	72.17	73.37	75.65	6.45	0.845

samples in the training set. Lawrence et al. (1996) suggested that good generalization is obtainable by using smaller network, which can fit the data well. Moreover, Urolagin et al. (2012) state that to obtain good generalization, the network should fit the data correctly while maintaining the possible smallest size. Therefore, we consider that the optimal number of neurons in the hidden layer is 10 except for time shift of 1, 2, 9, and 12 where the best number is 15, 5, 5, and 15 neurons, respectively. The weights and biases of the highest prediction performance ANNs of Table 1 are listed in Tables S1–S12. It should be also noted that the ANNs that have the highest prediction performance are also has the minimum RMSE for both the validation and test sets except the case of 10-hr shift.

Figure 4 presents the fitting between the predicted *Dst* and the real *Dst* values of the prediction set. With reference to equation (7), the figure shows the results of (a) *Dst* (N5,S2,D24), (b) *Dst* (N10,S4,D24), (c) *Dst* (N10,S6,D24), (d) *Dst* (N10,S8,D24), (e) *Dst* (N10,S10,D24), and (f) *Dst* (N15,S12,D24). These results indicate good prediction capabilities of the proposed ANNs. Moreover, The RMSE was estimated for different *Dst* ranges to estimate the ANN performance according to the *Dst* level. The RMSEs are presented in Figure 4 as vertical bars with 20-nT width. All the six ANNs presented in Figure 4 have RMSE less than 10 nT for *Dst* index values more than −40 nT. Meanwhile, the maximum RMSE was for *Dst* index level between −100 and −80 nT. However, the ANN forecasting the *Dst* 12 hr in advance has the least RMSEs for the different *Dst* levels except for *Dst* less than −120. Further, we investigate the ANN prediction performance through the strongest six geomagnetic storms observed during the prediction set period. Figure 5 illustrates the effectiveness of the trained ANNs to predict the *Dst* index 2, 6, and 12 hr ahead during geomagnetic storm periods. The statistical analysis of the ANN performance during these six storms is illustrated in Table 2.

The performance measures are ranging from 0.98 to 0.89, 14.3 to 6.5, and 11.6 to 4.3 nT for the *R*, RMSE, and MAE, respectively. The maximum and minimum *Dst* values observed during each event are given in the same table. Normally, geomagnetic storms have three phases, initial phase, main phase, and recovery phase (Gonzalez et al., 1994). The correlation coefficients during the main and recovery phases were estimated for the six storms of Figure 5 and are listed in Table 2. For comparison, the timing of the main and

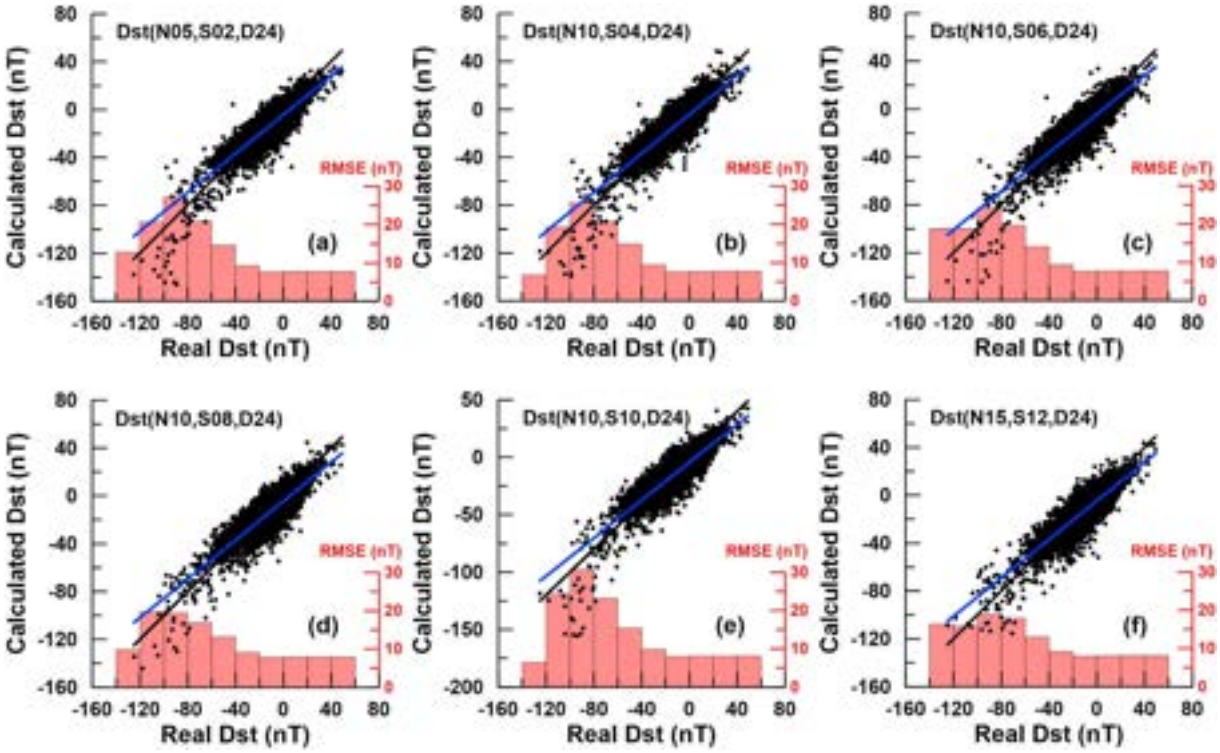

Figure 4. Comparison between the ANN calculated *Dst* (dot) and the real *Dst* (black line) values of the prediction set. The best fit between the real and predicted *Dst* is indicated by a blue line. (a) The *Dst* is calculated 2 hr in advance using ANN with five neurons. (b) *Dst* is estimated for time $t + 4$ using ANN with 10 neurons. (c) *Dst* for time $t + 6$ using ANN with 10 neurons. (d) *Dst* is estimated for time $t + 8$ using ANN with 10 neurons. (e) *Dst* is estimated for time $t + 10$ using ANN with 10 neurons. (f) Forecasting the *Dst* 12 hr in advance using ANN with 15 neurons in the hidden layer. The RMSE is presented for different *Dst* ranges as bars.

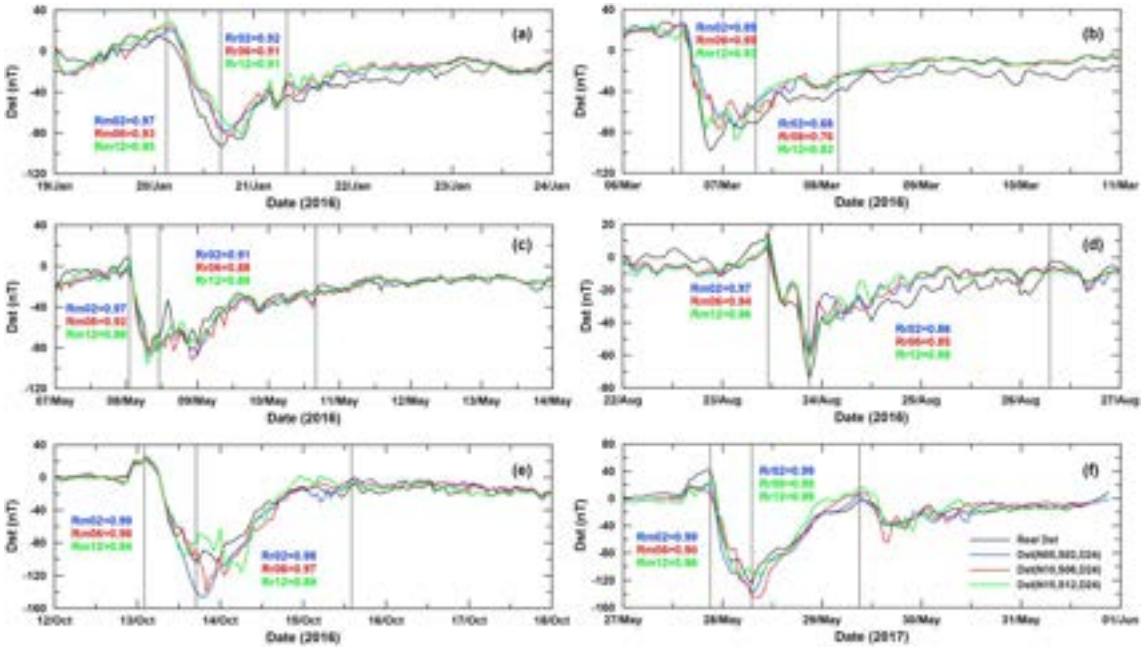

Figure 5. The accuracy of the proposed ANNs to forecast the *Dst* index 2, 6, and 12 hr ahead during the strongest six geomagnetic storms observed throughout the prediction set period. The vertical lines indicate the main and recovery phases.

Table 2
Statistical Analysis of Forecasting Result During Geomagnetic Storms

Event	Real *Dst* maximum/ minimum (nT)	Shift (hr)	*R*	RMSE (nT)	MAE (nT)	Maximum (nT)	Minimum (nT)	Main phase *R*	Recovery phase *R*
20–23 January 2016		2	0.95	9.86	8.05	21.49	−78.08	0.97	0.92
	16/−93	6	0.93	11.16	9.26	24.06	−81.79	0.93	0.91
		12	0.92	12.22	9.43	29.51	−82.07	0.95	0.91
6–10 March 2016		2	0.95	13.91	11.45	26.19	−75.25	0.89	0.68
	28/−98	6	0.96	13.60	11.69	25.49	−77.39	0.89	0.76
		12	0.96	12.72	11.68	26.46	−87.18	0.93	0.83
7–13 May 2016		2	0.96	7.53	5.40	−0.85	−88.15	0.97	0.91
	9/−83	6	0.94	8.78	6.09	−3.11	−91.68	0.92	0.88
		12	0.96	6.50	4.60	3.89	−95.49	0.98	0.89
22–26 August 2016		2	0.89	8.01	6.94	7.43	−58.58	0.97	0.86
	15/−74	6	0.89	7.78	6.53	5.31	−60.01	0.94	0.85
		12	0.89	7.95	6.82	10.99	−62.59	0.96	0.88
12–17 October 2016		2	0.98	12.79	8.31	26.30	−145.91	0.99	0.98
	26/−104	6	0.96	10.61	7.19	25.08	−139.34	0.98	0.97
		12	0.93	11.54	7.77	26.21	−115.58	0.94	0.89
27–31 May 2017		2	0.97	10.64	8.71	22.02	−137.84	0.99	0.99
	43/−125	6	0.93	14.30	10.80	18.05	−144.25	0.90	0.99
		12	0.94	12.00	9.63	26.32	−113.70	0.96	0.99

recovery phases for the first three storms are matched for that listed by Lazzús et al. (2017). These results indicate spectacular efficiency where the predicted *Dst* follow the real *Dst* variations and reproduce the initial, main, and recovery phases with a very similar pattern.

6. Solar Wind Parameter Geoeffectiveness

To investigate the *Dst* dependence on different solar wind parameters, we train the ANN with different parameter sets. Generally, SW input parameter matrix (equation (8)) can be considered in the form:

$$\mathrm{SW(L, d)}$$

where *L* is a selected group of the solar wind parameters set

$$\mathrm{L}\subseteq\{\mathrm{B}, \mathrm{B_z}, \mathrm{T}, \mathrm{D}, \mathrm{V}, \mathrm{P}, \mathrm{E}\}$$

and equation (7) can be rewritten in the form

$$Dst(L, N, S, d) = ANN[SW(L, d), N, S], \tag{9}$$

The ANN was trained using all possible subsets containing one to seven solar wind parameters. The number of all possible subsets is 127 sets. The number of different combinations of n distinct items taken *r* at a time is given by ${}_nC_r = \frac{n!}{r!(n-r)!}$. Therefore, beside the set of the 7 parameters, we have 7, 21, 35, 35, 21, and 7 subsets containing 1, 2, 3, 4, 5, and 6 parameters, respectively.

In this regard, we have seven subsets: each contains six solar wind parameters. These subsets are $L_1^6 = \{B, B_z, T, D, V, P\}$, $L_2^6 = \{B, B_z, T, D, V, E\}$, $L_3^6 = \{B, B_z, T, D, P, E\}$, $L_4^6 = \{B, B_z, T, V, P, E\}$, $L_5^6 = \{B, B_z, D, V, P, E\}$, $L_6^6 = \{B, T, D, V, P, E\}$, and $L_7^6 = \{B_z, T, D, V, P, E\}$.

Accordingly, the solar wind input matrix of the first six-parameter subset is

$$SW\left(L_1^6, d\right) = \begin{pmatrix} B(t) & B_z(t) & T(t) & D(t) & V(t) & P(t) \\ B(t-1) & B_z(t-1) & T(t-1) & D(t-1) & V(t-1) & P(t-1) \\ \vdots & \vdots & \vdots & \vdots & \vdots & \vdots \\ B(t-d) & B_z(t-d) & T(t-d) & D(t-d) & V(t-d) & P(t-d) \end{pmatrix}, \tag{10}$$

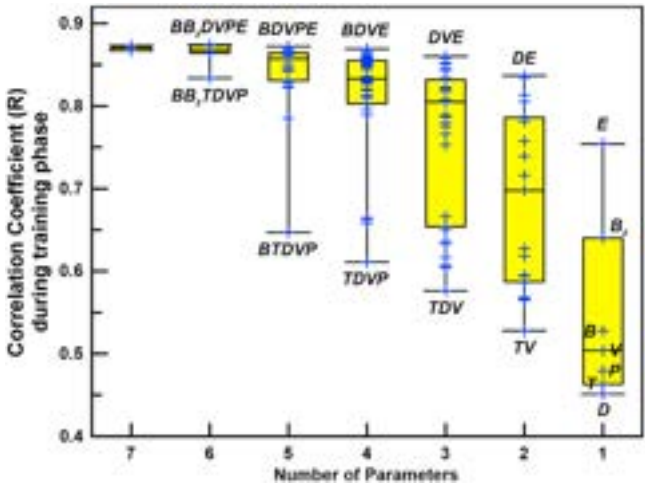

Figure 6. The prediction performance of ANNs trained with different solar parameter sets. The used ANN is used to predict the *Dst* 2 hr in advance using a delay of 24 data points. The ANN is trained using different parameter sets containing one parameter and up to seven parameters. In case of seven parameters, the ANN was trained several times.

Figure 6 shows the performance results of the training phase of ANNs trained with different solar parameter sets containing one parameter and up to seven parameters. Additionally, Figure 6 shows the maximum, mean, minimum, and whisker box (first and third quartiles) of each ANN group trained with the same number of parameters. Considering the mean and the whisker box, generally, the forecasting performance decreases with reducing the number of parameters. However, the maximum values of *R* are 0.873, 0.874, 0.872, 0.869, 0.860, 0.837, and 0.754 for number of parameters from 7 to 1, respectively. The results of the ANN obtaining the maximum performance at each number of parameters are listed in Table 3. Remarkably, the highest training performance was achieved using six parameters only while the highest performance achieved during the prediction phase was using the whole seven parameters.

Logically, removing any parameter from the input matrix may produce a shortage in the knowledge presented to the ANN. However, when considering the contribution of every single parameter to the overall performance, it could be indicated that the *E* is the most significant (as it always contribute to the maximum performance). Meanwhile, the most irrelevant is not clear; for example, *D* is contributing to both maximum and minimum values. Interestingly, *D* appears to have the minimum performance for a single input parameter and contributes to the maximum performance when combined with *E*. Therefore, *D* appears to have a complementary or necessary information. Additionally, as noted from Table 3, the highest training performance was achieved using only six parameters (B, B_z, D, V, P, E) that does not contain the temperature. Moreover, the temperature is contributing to the minimum performance for input sets of two to six parameters. Therefore, we could state that the temperature appears to be more irrelevant parameter when combined with other parameters and *D* appears to be more significant when combined with other parameters.

However, the second significant parameter is B_z. This is clear in case of single-parameter input. In addition, in case of five parameters, the only input set that does not contain E and B_z has the minimum *R*. The rest of the parameters (B, T, D, V, and P) may have matching ranks.

7. The Effect of the Training Period

To assist how the results of the ANNs will generalize to an independent input data set we perform cross-validation test. The training set was divided into 10 blocks. One block was used for ANN testing. While, the following and preceding block or the following or the preceding two blocks were used for validations and the remaining seven blocks were used for learning. The performance results during the training and

Table 3
Performance of the ANN Obtaining the Maximum R During Training

Solar wind input		Training phase						Prediction phase		
		Training set			Learning	Validation	Test			
RMSE (nT)	MAE (nT)	*R*	RMSE (nT)	RMSE (nT)	RMSE (nT)	RMSE (nT)	MAE (nT)	*R*	*n*	Parameters
7	B, B_z T, D, V, P, E	57.16	5.63	0.873	55.89	59.55	60.73	62.70	6.08	0.876
6	B, B_z, D, V, P, E	60.12	5.79	0.874	59.31	62.66	61.36	67.04	6.23	0.874
5	B, D, V, P, E	60.95	5.79	0.872	59.54	63.56	64.91	63.55	6.06	0.873
4	B, D, V, E	62.32	5.83	0.869	60.46	66.07	67.25	66.47	6.24	0.872
3	D, V, E	66.37	5.98	0.860	64.91	70.44	69.12	68.19	6.25	0.863
2	D, E	76.02	6.39	0.837	74.48	80.15	79.04	71.46	6.39	0.839
1	E	109.92	7.80	0.754	108.62	109.62	116.24	106.35	7.95	0.748

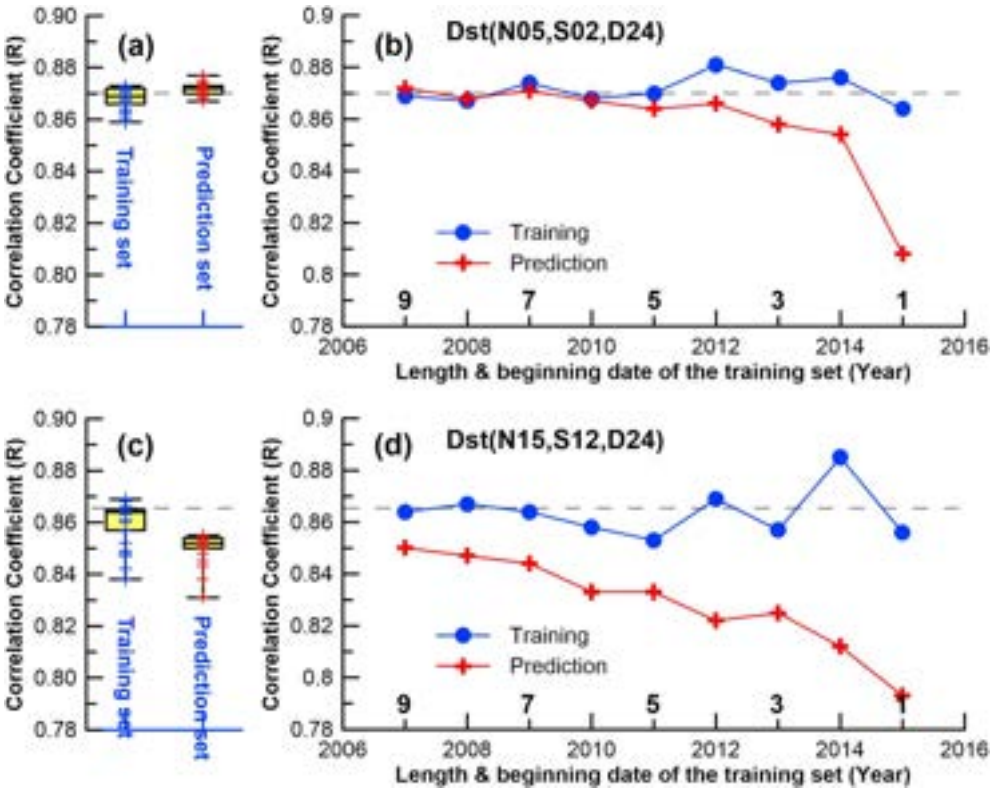

Figure 7. The training and prediction performance of 2 and 12 hr forecasting for ANNs trained with different learning sets. (a) Two-hour ahead prediction. (b) Twelve-hour ahead prediction. The horizontal dashed line represents the corresponding value of training performance *R* listed in Table 1.

prediction phases are shown in Figures 7a and 7c for 2- and 12-hr ahead forecasting. The 2 hr in advance predictions has maximum training performance $R = 0.874$ and the minimum is $R = 0.859$ with mean value $R = 0.868$ (0.002 less than what is listed in Table 1) and standard deviation 0.0038. Meanwhile, the prediction performance has a maximum $R = 0.878$ and minimum $R = 0.867$ and mean value $R = 0.872$ (0.002 less than what is listed in Table 1) and standard deviation 0.0025. Likewise, the 12 hr in advance predictions has maximum training performance $R = 0.869$ and the minimum is $R = 0.838$ with mean value $R = 0.859$ (0.006 less than what is listed in Table 1) and standard deviation 0.0087. Meanwhile, the prediction performance has a maximum $R = 0.855$ and minimum $R = 0.831$ and mean value $R = 0.850$ (0.007 less than what is listed in Table 1) and standard deviation 0.0055. The low standard deviation values indicate that the results do not depend on the input training set.

Furthermore, the effect of the size of the training set on the ANN performance was investigated by reducing the size of the training set. Figures 7b and 7d show the training and prediction performance for different training sets. The size of the training set was reduced one year per time. The minimum training set was one year long from 1 January 2015 to 31 December. The training performance for both 2- and 12-hr ahead forecasting remains within the range (as shown by Figures 7a and 7b). However, the prediction performance *R* shows some reduction. For 2-hr forecasting the prediction performance is decreasing for training sets less than four years long. This reduction in the prediction performance indicates that a short training set of three years or less contains insufficient number of samples that cannot allow the ANN to achieve good generalization. Meanwhile, for the 12-hr ahead prediction the performance is improving with longer training sets.

8. Discussion and Conclusion

We succeed to train the ANN with solar wind data to achieve forecasting of the *Dst* index up to 12 hr in advance. The number of neurons was gradually increased with increasing the size of the input vector

Table 4
Comparison of the Results Obtained by the Proposed Method and Lazzús et al. (2017) Method

	Proposed method		Lazzús et al. (2017)	
Event	Main phase R	Recovery phase R	Main phase R	Recovery phase R
January 2016	0.97	0.92	0.88	0.87
March 2016	0.89	0.68	0.89	0.86
May 2016	0.97	0.91	0.95	0.89

represented by the delay time. The best performance was achieved using 10 neurons in the hidden layer except for time shift of 1, 2, 9, and 12 where the best number of neurons was 15, 5, 5, and 15, respectively. The time delay was 24 hr, except for time shift of 1 hr, it was 9-hr delay. Generally, the proposed technique has a good accuracy for forecasting the *Dst* index for 2 to 12 hr in advance. The performance measure *R* was ranging from 0.886 to 0.870 during the training phase. Meanwhile, *R* was ranging from 0.874 to 0.857 during the prediction phase.

The forecast performance according to the *Dst* index level was presented in Figure 4. Generally, the RMSE is less than 10 nT for *Dst* index values more than −40 nT. Meanwhile, the maximum RMSE for *Dst* index level between −100 and −80 nT is about 30 nT. However, the ANN forecasting the *Dst* 12 hr in advance has the least RMSEs for the different *Dst* levels except for *Dst* less than −120. Comparably with the prediction set *Dst* levels (Figure 1), 96.4% of the data has RMSE less than 10 nT.

Moreover, the capability of the proposed method to forecast that the storm phase was investigated through the strongest six geomagnetic storms occurs during the prediction set period. The maximum correlation coefficient during the main phase was 0.99 and the minimum was 0.89. Meanwhile, during the recovery phase, the maximum correlation coefficient was 0.99 and the minimum was 0.68. The three events of January, March, and May 2016 were used by Lazzús et al. (2017) for *Dst* forecasting. Table 4 represents the results of Lazzús et al. (2017) for 2 hr in advance forecast against the proposed method.

To signify the advantage of our proposed method for forecasting 12 hr in advance over previously published methods, we summarize some the results of these methods. Table 5 shows a comparison between Wu and Lundstedt (1997) Elman ANN, Lazzús et al. (2017), and our proposed ANN. Wu and Lundstedt (1997) predict the *Dst* index for 3 to 8 hr ahead with *R* equal to 0.88, 0.86, 0.84, 0.82, 0.80, and 0.77, respectively. The correlation coefficient for Wu and Lundstedt (1997) Elman ANN is high for 1- to 3-hr ahead forecasting and reduce for longer prediction time. This high prediction performance is a direct consequence of the increased dynamic of the Elman network where it uses feedback connections (context units) which acts as an additional input. However, our ANN models use longer time delay (24 hr) and more parameters (seven parameters); therefore, it was able to predict *Dst* for 4 to 12 hr ahead with higher performance.

Lazzús et al. (2017) obtain prediction for 3 to 6 hr in advance with *R* equal to 0.895, 0.857, 0.825, and 0.788, respectively. In addition, Ji et al. (2012) presented a comparison between six *Dst* forecasting models. The

Table 5
Comparison Between Wu and Lundstedt (1997), Lazzús et al. (2017), and Our Proposed ANN Results

	Wu and Lundstedt (1997)	Proposed method	Lazzús et al. (2017)
Shift (hr)	*R*	*R*	*R*
1	0.92	0.845	0.978
	0.92		
2	0.92	0.874	0.936
	0.90		
3	0.88	0.872	0.895
4	0.86	0.869	0.857
5	0.84	0.865	0.825
6	0.82	0.864	0.788
7	0.80	0.862	
8	0.77	0.860	
9		0.860	
10		0.857	
11		0.860	
12		0.857	

Note: ANN = artificial neural network.

average correlation coefficients over 139 geomagnetic storms were between 0.77 and 0.88 for the six models for 1 hr in advance forecasting. The proposed model has low performance for 1-hr forecasting; however, the main target was to achieve longer prediction time. Therefore, 0- and 1-hr prediction was performed using 1- to 9-hr delay as presented in Figure 2.

This medium-term prediction of 12 hr in advance could be used for alarm and early warning systems. However, the solar wind parameters are not all of the same significant in relation to geomagnetic activities. Our results show that the solar wind electric field is the most significant parameter while the second is the southward IMF component B_z. This result is in agreement with Khabarova et al.'s (2006) work, where they state that E has a slightly higher significance than B_z. However, different combinations of the solar wind parameters have a slightly different significant. The temperature appears to be more irrelevant parameter when combined with other parameters and *D* appears to be more significant when combined with other parameters.

This study indicates that the solar wind density has a more significant geoeffective role than was previously supposed. The significance of the combined parameters may indicate that they complement each other in their interaction with the magnetosphere through variations in both parameters. The geoeffectiveness of *D* and *E* as input set suggests that *D* has triggering role in the *Dst* index variations and consequently geomagnetic storms. Borovsky (2016) point out that large-scale *E* has its source in the distributed charge density in the solar wind plasma.

Acknowledgments
The list of SSC is calculated and made available by ISGI Collaborating Institutes from data collected at magnetic observatories. We thank the involved national institutes, the INTERMAGNET network, and ISGI. We also acknowledge the use of NASA/GSFC's Space Physics Data Facility's OMNIWeb service and OMNI data.

References

Akasofu, S.-I. (1981). Prediction of development of geomagnetic storms using the solar wind-magnetosphere energy coupling function epsilon. *Planetary and Space Science*, *29*(11), 1151–1158.

Borovsky, J. E. (2016). Relativity and the solar wind: The Maxwell-equation origins of the solar-wind motional electric field. *Journal of Electromagnetic Analysis and Applications*, *8*(08), 133–151. https://doi.org/10.4236/jemaa.2016.88014

Boynton, R., Balikhin, M., Billings, S., Sharma, A., & Amariutei, O. (2011). Data derived NARMAX *Dst* model. *Annales Geophysicae*, *29*(6), 965–971 . https://doi.org/10.5194/angeo-29-965-2011

Burton, R. K., McPherron, R. L., & Russull, C. (1975). An empirical relationship between interplanetary conditions and *Dst*. *Journal of Geophysical Research*, *80*, 4202–4214.

Caswell, J. (2014). A nonlinear autoregressive approach to statistical prediction of disturbance storm time geomagnetic fluctuations using solar data. *Journal of Signal and Information Processing*, *5*(02), 42–53. https://doi.org/10.4236/jsip.2014.52007

Curto, J. J., Card'us, J. O., Alberca, L. F., & Blanch, E. (2007). Milestones of the IAGA International Service of Rapid Magnetic Variations and its contribution to geomagnetic field knowledge. *Earth, Planets and Space*, *59*(5), 463–471.

Gleisner, H., Lundstedt, H., & Wintoft, P. (1996). Predicting geomagnetic storms from solar wind data using time-delay neural networks. *Annales de Geophysique*, *14*(7), 679–686.

Gonzalez, W. D., Dal Lago, A., Clúa de Gonzalez, A. L., Vieira, L. E. A., & Tsurutani, B. T. (2004). Prediction of peak-*Dst* from halo CME/magnetic cloud-speed observations. *Journal of Atmospheric and Solar-Terrestrial Physics*, *66*(2), 161–165. https://doi.org/10.1016/j.jastp.2003.09.006

Gonzalez, W. D., & Echer, E. (2005). A study on the peak *Dst* and peak negative B_z relationship during intense geomagnetic storms. *Geophysical Research Letters*, *32*, L18103. https://doi.org/10.1029/2005GL023486

Gonzalez, W. D., Joselyn, J. A., Kamide, Y., Kroehl, H. W., Rostoker, G., Tsurutani, B. T., & Vasyliunas, V. M. (1994). What is a geomagnetic storm? *Journal of Geophysical Research*, *99*(A4), 5771–5792. https://doi.org/10.1029/93JA02867

Huang, G.-B., & Babri, H. A. (1998). Upper bounds on the number of hidden neurons in feedforward networks with arbitrary bounded nonlinear activation functions. *IEEE Transactions on Neural Networks*, *9*(1), 224–229.

Huang, S. C., & Huang, Y. F. (1991). Bounds on the number of hidden neurons in multilayer perceptrons. *IEEE Transactions on Neural Networks*, *2*(1), 47–55.

Ji, E.-Y., Moon, Y.-J., Gopalswamy, N., & Lee, D.-H. (2012). Comparison of *Dst* forecast models for intense geomagnetic storms. *Journal of Geophysical Research*, *117*, A03209. https://doi.org/10.1029/2011JA016872

Khabarova, O., Pilipenko, V., Engebretson, M. J., & Rudenchik, E. (2006). Solar wind and interplanetary magnetic field features before the magnetic storm onset. In *Proc. Int. Conf. Substorms-8* (pp. 1–6). Canada: Banff Centre.

Kim, R.-S., Moon, Y.-J., Gopalswamy, N., Park, Y.-D., & Kim, Y.-H. (2014). Two-step forecast of geomagnetic storm using coronal mass ejection and solar wind condition. *Space Weather*, *12*, 246–256. https://doi.org/10.1002/2014SW001033

King, J. H., & Papitashvili, N. E. (2005). Solar wind spatial scales in and comparisons of hourly wind and ACE plasma and magnetic field data. *Journal of Geophysical Research*, *110*, A02104. https://doi.org/10.1029/2004JA010649

Kosko, B. (1992). *Neural networks and fuzzy systems*. Englewood Ciffs, NJ: Prentice Hall.

Kugblenu, S., Taguchi, S., & Okuzawa, T. (1999). Prediction of the geomagnetic storm associated *Dst* index using an artificial neural network algorithm. *Earth, Planets and Space*, *51*(4), 307–313. https://doi.org/10.1186/BF03352234

Lawrence, S., Giles, C. L., & Tsoi, A. C. (1996). What size neural network gives optimal generalization? Convergence properties of back propagation. Technical Report, UMIACS-TR-96-22 and CS-TR-3617 (pp. 20742). College Park, MD: Institute for Advanced Computer Studies, University of Maryland.

Lawrence, S., & Giles, L. C. (2000). Overfitting and neural networks: Conjugate gradient and backpropagation. In: IEEE IJCNN (pp. 114–119). Italy, CA, July 24-27.

Lazzús, J. A., L'opez-Caraballo, C. H., Rojas, P., Salfate, I., Rivera, M., & Palma-Chilla, L. (2014). Forecasting of *Dst* index from auroral electrojet indices using time-delay neural network + particle swarm optimization. *Journal of Physics: Conference Series*, *720*, 012001. https://doi.org/10.1088/1742-6596/720/1/012001

Lazzús, J. A., Vega, P., Rojas, P., & Salfate, I. (2017). Forecasting the *Dst* index using a swarm-optimized neural network. *Space Weather*, *15*, 1068–1089. https://doi.org/10.1002/2017SW001608
Levenberg, K. (1944). A method for the solution of certain problems in least squares. *Quarterly of Applied Mathematics*, *5*, 164–168.
Li, X., Oh, K. S., & Temerin, M. (2007). Prediction of the *AL* index using solar wind parameters. *Journal of Geophysical Research*, *112*, A06224. https://doi.org/10.1029/2006JA011918
Lundstedt, H., & Wintoft, P. (1994). Prediction of geomagnetic storms from solar wind data with the use of a neural network. *Annales de Geophysique*, *12*(1), 19–24.
MacDonald, N. J., & Ward, F. (1963). The prediction of geomagnetic disturbance indices: 1. The elimination of internally predictable variations. *Journal of Geophysical Research*, *68*(11), 3351–3373. https://doi.org/10.1029/JZ068i011p03351
Marquardt, D. (1963). An algorithm for least-squares estimation of nonlinear parameters. *SIAM Journal on Applied Mathematics*, *11*(2), 431–441. https://doi.org/10.1137/0111030
Masahito, N., Masahisa, S., Toyohisa, K., Toshihiko, I., & Yukinobu, K. (2015). *Dst* index (version 1.0). WDC for Geomagnetism, Kyoto. https://doi.org/10.17593/14515-74000
Mayaud, P. N. (1973). *A Hundred Year Series of Geomagnetic Data, 1868–1967: Indices aa, Storm Sudden Commencements (SSC)* (p. 256). Paris: IUGG Publ. Office.
Mays, M. L., Horton, W., Spencer, E., & Kozyra, J. (2009). Real-time predictions of geomagnetic storms and substorms: Use of the solar wind magnetosphere-ionosphere system model. *Space Weather*, *7*, S07001. https://doi.org/10.1029/2008SW000459
Meen, T.-H., Prior, S., & Lam, A. D. K.-T. (2015). Innovation in design, communication and engineering, Proceedings of the 3rd International Conference on Innovation, Communication and Engineering (ICICE 2014), Guiyang, Guizhou, P.R. China, October 17–22, 2014.
Mirko, B., & Christain, J. (2000). Neural networks in geophysical applications. *Geophysics*, *65*, 1032–1047.
Nikolaeva, N. S., Yermolaev, Y. I., & Lodkina, I. G. (2014). Dependence of geomagnetic activity during magnetic storms on the solar wind parameters for different types of streams: 4. Simulation for magnetic clouds. *Geomagnetism and Aeronomy*, *54*(2), 152–161.
O'Brien, T. P., & McPherron, R. L. (2000). Forecasting the ring current index *Dst* in real time. *Journal of Atmospheric and Solar - Terrestrial Physics*, *62*, 1295–1299.
Pallocchia, G., Amata, E., Consolini, G., Marcucci, M. F., & Bertello, I. (2006). Geomagnetic *Dst* index forecast based on IMF data only. *Annales de Geophysique*, *24*(3), 989–999.
Perreault, W. K., & Akasofu, S.-I. (1978). A study of geomagnetic storms. *Geophysical Journal of the Royal Astronomical Society*, *54*(3), 547–573.
Poulton, M. M., Sternberg, B. K., & Glass, C. E. (1992). Location of subsurface targets in geophysical data using neural networks. *Geophysics*, *57*(12), 1534–1544. https://doi.org/10.1190/1.1443221
Qin, P., & Nishii, R. (2015). Statistical prediction of *Dst* index by solar wind data and *t*-distributions. *IEEE Transactions on Plasma Science*, *43*(11), 3908–3915. https://doi.org/10.1109/TPS.2015.2485661
Rastätter, L., Kuznetsova, M. M., Glocer, A., Welling, D., Meng, X., Raeder, J., et al. (2013). Geospace environment modelling 2008–2009 challenge: *Dst* index. *Space Weather*, *11*, 187–205. https://doi.org/10.1002/swe.20036
Reed, R. D., & Marks, R. J. II (1999). *Neural Smithing*. Cambridge, MA: MIT Press.
Schalkoff, R. (1997). *Artificial Neural Networks*. New York: McGraw-Hill.
Smith, S. (1997). *The Scientist and Engineer's Guide to Digital Signal Processing*. San Diego, CA: California Technical Publishing.
Sugiura, M. (1964). *Hourly Values of Equatorial Dst* for IGY, *Ann. Int. Geophys. Year* (Vol. 35, p. 9). Oxford: Pergamon Press.
Sugiura, M. (1969). IAGA resolution 2, in: IAGA bulletin 27 (p. 123). Madrid.
Sugiura, M., & Chapman, S. (1960). *The Average Morphology of Geomagnetic Storms With Sudden Commencement*, Abandl. Akad. Wiss., Göttingen: Vandenhoeck & Ruprecht, Math. Phys. K1 (4).
Sugiura, M., & Kamei, T. (1991). Equatorial *Dst* index 1957–1986, IAGA Bulletin No. 40.
Temerin, M., & Li, X. (2002). A new model for the prediction of *Dst* on the basis of the solar wind. *Journal of Geophysical Research*, *107*(A12), 1472. https://doi.org/10.1029/2001JA007532
Urolagin, S., Prema, K. V., & Reddy, N. (2012). Generalization capability of artificial neural network incorporated with pruning method. *Lecture Notes in Computer Science*, 171–178. https://doi.org/10.1007/978-3-642-29280-4_19
Uwamahoro, J., & Habarulema, J. B. (2014). Empirical modeling of the storm time geomagnetic indices: A comparison between the local *K* and global *Kp* indices. *Earth, Planets and Space*, *66*(1), 95. https://doi.org/10.1186/1880-5981-66-95
Watanabe, S., Sagawa, E., Ohtaka, K., & Shimazu, H. (2002). Prediction of the *Dst* index from solar wind parameters by a neural network method. *Earth, Planets and Space*, *54*(12), 1263–1275. https://doi.org/10.1186/BF03352454
Watari, S. (2017). Geomagnetic storms of cycle 24 and their solar sources. *Earth, Planets and Space*, *69*(1). https://doi.org/10.1186/s40623-017-0653-z
Wu, J.-G., & Lundstedt, H. (1996). Prediction of geomagnetic storms from solar wind data using Elman recurrent neural networks. *Geophysical Research Letters*, *23*(4), 319–322.
Wu, J.-G., & Lundstedt, H. (1997). Geomagnetic storm predictions from solar wind data with the use of dynamic neural networks. *Journal of Geophysical Research*, *102*(A7), 14,255–14,268. https://doi.org/10.1029/97JA00975
Yermolaev, Y. I., Lodkina, I. G., Nikolaeva, N. S., & Yermolaev, M. Y. (2013). Occurrence rate of extreme magnetic storms. *Journal of Geophysical Research: Space Physics*, *118*, 4760–4765. https://doi.org/10.1002/jgra.50467
Yermolaev, Y. I., Nikolaeva, N. S., Lodkina, I. G., & Yermolaev, M. Y. (2010). Specific interplanetary conditions for CIR-, sheath-, and ICME-induced geomagnetic storms obtained by double superposed epoch analysis. *Annales Geophysicae*, *28*(12), 2177–2186.
Yermolaev, Y. I., & Yermolaev, M. Y. (2002). Statistical relationships between solar, interplanetary, and geomagnetospheric disturbances, 1976–2000. *Cosmic Research*, *40*(1), 1–14.
Yermolaev, Y. I., Yermolaev, M. Y., Zastenker, G. N., Zelenyi, L. M., Petrukovich, A. A., & Sauvaud, J.-A. (2005). Statistical studies of geomagnetic storm dependencies on solar and interplanetary events: A review. *Planetary and Space Science*, *53*, 189–186. https://doi.org/10.1016/j.pss.2004.09.044